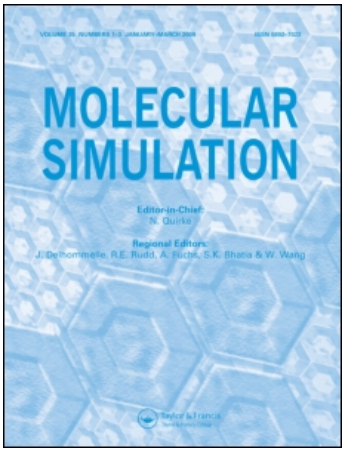

Molecular Simulation

Publication details, including instructions for authors and subscription information:
http://www.informaworld.com/smpp/title~content=t713644482

Nonequilibrium molecular dynamics simulation for size effects on thermal conductivity of Si nanostructures

Y. W. Yang[a]; X. J. Liu[ab]; J. P. Yang[b]
[a] School of Civil and Environmental Engineering, Nanyang Technological University, Singapore [b] Data Storage Institute, Singapore

To cite this Article Yang, Y. W. , Liu, X. J. and Yang, J. P.(2008) 'Nonequilibrium molecular dynamics simulation for size effects on thermal conductivity of Si nanostructures', Molecular Simulation, 34: 1, 51 — 56
To link to this Article: DOI: 10.1080/08927020701730419
URL: http://dx.doi.org/10.1080/08927020701730419

Molecular Simulation
Vol. 34, No. 1, January 2008, 51–55

Taylor & Francis
Taylor & Francis Group

Nonequilibrium molecular dynamics simulation for size effects on thermal conductivity of Si nanostructures

Y.W. Yang[a]*, X.J. Liu[ab1] and J.P. Yang[b2]

[a]*School of Civil and Environmental Engineering, Nanyang Technological University, Nanyang Avenue, 639798 Singapore;* [b]*Data Storage Institute, DSI Building, 5 Engineering Drive 1, 117608, Singapore*

(Received 12 August 2007; final version received 6 October 2007)

The thermal conductivity of Si nanostructres is investigated using nonequilibrium molecular dynamics (NEMD) simulation based on the Tersoff III inter-atomic potential. A reliable range of heat flux for the calculation of thermal conductivity is determined by the comparative study of NEMD simulations with different heat fluxes. The remarkable dependence of thermal conductivity on the length of nanostructures is observed. It is also found that the thermal conductivity is less sensitive to the cross-section area perpendicular to the heat flux than to the length of Si nanostructures. Based on the relationship between the thermal conductivity and the nanostructure length, the thermal conductivity and the phonon mean-free path of the infinite bulk Si system are extrapolated.

Keywords: nanostructure; molecular dynamics simulation; thermal conductivity; NEMS/MEMS

1. Introduction

Thermal characterization of nanostructures is a fundamental issue for the reliability of nano/micro-electro-mechanical systems (NEMS/MEMS), especially, the thermoelectric effect based energy conversion systems. In these systems, when the size of nanostructures becomes comparable to the inter-atomic distances, their thermal conductivity will be greatly scale-dependent. However, the measurement of thermal conductivity for nanostructures remains difficult because the influence of experiment environment and individual defects, such as impurities, grain boundaries and others, cannot be fully controlled and clearly analyzed. On the other hand, nonequilibrium molecular dynamics (NEMD) simulation method is an ideal tool for addressing such issues, which is analogous to the experimental situation by imposing a temperature gradient and a heat flux across the system. With theoretical analysis and numerical simulation, the NEMD method can provide insight of nanoscale heat transfer phenomenon.

Since crystalline Si is widely used in NEMS/MEMS, the thermal properties of Si nanostructures are investigated in this paper. For the perfect crystal Si, or the intrinsic and moderately doped Si, the heat transfer due to electrons and radiation is negligible compared to the phonon heat transfer. Several inter-atomic potentials have been proposed for the NEMD simulation of Si material [1]. Compared with other potentials, such as the Stillinger–Weber (SW) potential [2], the Harrison potential [3], and the Biswas and Hamann potential [4], the N-body Tersoff III (T3) potential [5], taking into account the local environment surrounding the bonds, is able to produce more accurate results when simulating the characteristic surface structures, the low-coordination-number geometries and the high-pressure polymorphs with both the standard and unconventional geometries [6]. This is desirable for the accurate simulation of NEMS/MEMS devices or nanostructures with unconventional geometries. Therefore, the Tersoff potential is selected to simulate the nanoscale Si structures in this paper.

The rest of paper is organized as follows. In the next section, the NEMD simulation method and its application to the calculation of thermal conductivity are presented. In the third section, a reliable range of heat flux is determined to obtain the thermal conductivity of the Si nanostructures. The fourth section reports the simulation results with discussion on the finite-size effects on the thermal conductivity of Si nanostructures, followed by the conclusions in the last section.

2. NEMD simulation for thermal conductivity

The NEMD simulation method numerically mimics a guarded hot plate experiment. The "experiment" system includes a hot thermal reservoir, a cold thermal reservoir, and a sample to be studied which is placed between the hot and cold thermal reservoirs. The hot

*Corresponding author. Email: cywyang@ntu.edu.sg

ISSN 0892-7022 print/ISSN 1029-0435 online

DOI: 10.1080/08927020701730419
http://www.informaworld.com

and cold thermal reservoirs, consisting of thermostatted sets of atoms, are used to create a temperature gradient in the system, as shown in Figure 1. Upon the creation of these hot and cold regions, it is possible to control the energy imported into or taken from the thermal reservoirs by rescaling the atom velocity fields of the hot and cold reservoirs. With this method, the heat flux can be perfectly controlled to keep constant during the simulation.

In this study, the size of the sample is defined by $N_x a_0 \times N_y a_0 \times N_z a_0$ where the Si lattice constant a_0 is equal to 0.5431 nm, and N_x, N_y and N_z are the numbers of lattices in the x, y and z directions respectively. The mass density of the Si atoms is $\rho = 2.329\,\mathrm{g/cm^3}$. The hot and cold thermal reservoirs consist of sets of atoms forming a slice parallel to the xy plane so that heat transfer is unidimensional in the z direction. The hot and cold thermal reservoirs can be located anywhere in the sample, but the distance between them should be a half-length of the sample because of the periodic boundary condition (PBC), as shown in Figure 1.

The thermal conductivity relates the heat flux to the temperature gradient via the Fourier's law as follows

$$k(T) = -\frac{J_z}{\nabla T_z} \tag{1}$$

$$J_z = \left(\frac{\Delta\varepsilon}{A \cdot \Delta t}\right), \tag{2}$$

where k is the thermal conductivity; J_z is the heat flux defined as the amount of heat energy ($\Delta\varepsilon$) transferred per unit time (Δt) through unit area (A) perpendicular to the direction of the heat flux; and $\nabla T_z = \partial T/\partial z$ is the temperature gradient in the z direction, which is calculated using the NEMD simulation.

To calculate the temperature gradient, the simulation system is divided into j slices along the z direction. The temperatures of all slices are calculated in each iteration. The instantaneous temperature in each slice of the system

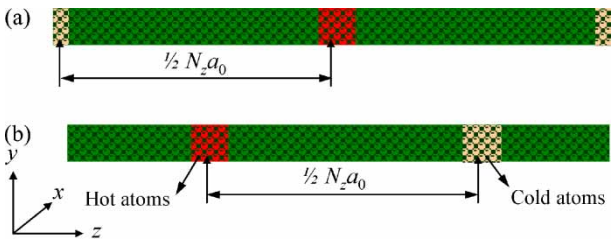

Figure 1. Geometric configuration of samples for PBC. The red represents hot region while the yellow represents cold region.

centred at position z can be obtained as

$$T_j(t)\frac{\left\langle \sum_{i=1}^{N_j} m_i v_i^2 \right\rangle}{3N_j k_B}, \tag{3}$$

where $T_j(t)$ is the temperature in the jth slice; m_i and v_i are the mass and velocity of the ith atom in the jth slice, respectively; $\langle\,\rangle$ denotes the statistical average over the entire simulation period; N_j is the number of atoms in the jth slice; and k_B is the Boltzman constant.

After the system reaches at the equilibrium status, a heat flux is imposed on the system along the z direction. A small amount of kinetic energy, $\Delta\varepsilon$, is added in the hot thermal reservoir. Simultaneously, the same amount of energy is removed from the cold thermal reservoir. To modify the temperature of the hot/cold reservoirs due to the addition/removal of $\Delta\varepsilon$, the velocity of each atom in the reservoirs is rescaled by a factor α, as

$$\alpha^2 = 1 \pm \frac{2\Delta\varepsilon}{\sum_{i=0}^{n_r} m_i \cdot v_{i\_\mathrm{old}}^2} \tag{4}$$

$$v_{i\_\mathrm{new}} = \alpha \cdot v_{i\_\mathrm{old}}, \tag{5}$$

where n_r is the number of atoms in the hot/cold reservoirs; and v_{i_old} and v_{i_new} are the velocities of the ith atom before and after rescaling, respectively.

3. Influence of heat flux on thermal conductivity

The NEMD involves in large temperature gradient ($\approx 10^9$ K/m), which is well beyond the experimental range. This large temperature gradient may introduce significant nonlinear response effects so that the Fourier's law is no longer applicable. In order to ensure the linear response effects in the thermal transfer so that the Fourier's law, is still obeyed for the simulated nanostructures, it is necessary to identify the range of heat energy variation $\Delta\varepsilon$ where the thermal conductivity k does not exhibit large variations. To achieve this, we performed the NEMD simulations with different $\Delta\varepsilon$ for a $3a_0 \times 3a_0 \times 44a_0$ sample at $T = 500$ K with the PBC. As shown in Equation (2), the heat flux J_z is proportional to $\Delta\varepsilon/A$, where $A = 2.654\,\mathrm{nm^2}$ for the $3a_0 \times 3a_0 \times 44a_0$ sample. The step time Δt is set as 0.57 fs, which is short enough to resolve the vibrational motions of the Si atoms. The simulated temperature profiles of the sample with different $\Delta\varepsilon$ are illustrated in Figure 2. The influence of the heat flux on the thermal conductivity k is shown in Figure 3.

It can be found that both the temperature profiles and the thermal conductivity vary with $\Delta\varepsilon$. However, in Figure 3, for $\Delta\varepsilon/A$ in the range of $1.0 \sim 7.0 \times 10^{-4}\,\mathrm{eV/nm^2}$ (corresponding to $\Delta\varepsilon = 2.654 \sim 18.582 \times 10^{-4}\,\mathrm{eV}$ for the sample with $A = 2.654\,\mathrm{nm^2}$),

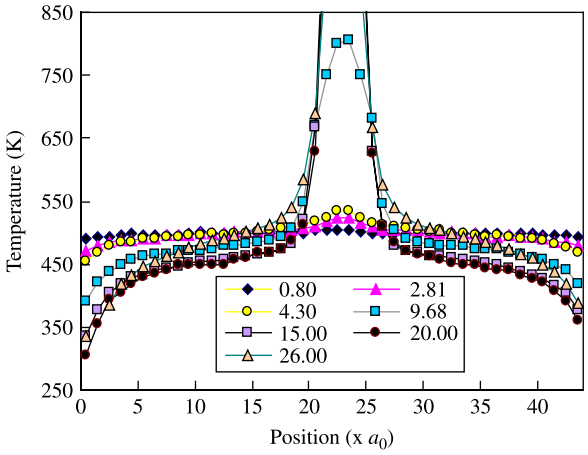

Figure 2. Temperature profile for $3a_0 \times 3a_0 \times 44a_0$ at $T = 500$ K for different $\Delta\varepsilon$: (0.80, 2.81, 4.30, 9.68, 15.00, 20.00, 26.00) $\times 10^{-4}$ eV.

the variations of k are smaller than 10%, implying that a relatively accurate value of k can be calculated within this range. This range covers those employed in previous researches using the SW potential, where $\Delta\varepsilon/A \approx 1.06 \times 10^{-4}$ eV/nm^2 in [7] and 1% of k_BT/A in [8]. It can be a useful guideline for choosing a suitable value of $\Delta\varepsilon/A$ to simulate the Si nanostructures/devices with unconventional geometries.

It is further observed in Figure 3 that selection of $\Delta\varepsilon/A$ significantly smaller than 1×10^{-4} eV/nm^2 tends to result in large error bars. It is because the magnitude of the temperature difference between the hot and cold reservoirs becomes comparable to the typical statistical noise. On the other hand, although no significant deviation from the Fourier's law appears when $\Delta\varepsilon/A > 7.0 \times 10^{-4}$ eV/nm^2, large values of $\Delta\varepsilon/A$ should be avoided for accuracy. With the increase of

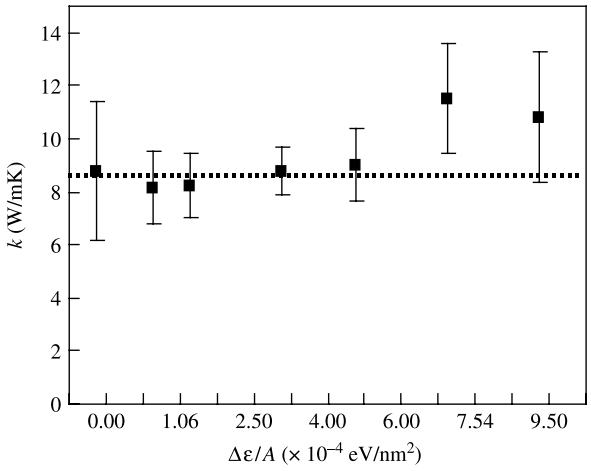

Figure 3. Thermal conductivity k with change of $\Delta\varepsilon/A$ for $3a_0 \times 3a_0 \times 44a_0$ at $T = 500$ K.

Table 1. Comparison of thermal conductivity k for various system length l_z.

l_z ($\times a_0$)	∇T_z (*K/nm*)	k (*W/mK*)	k' (W/mK; results in literature)
44	4.48	11.44	8.07 [12]
64	3.16	16.23	–
84	2.82	18.16	–
104	2.09	24.57	–
124	1.85	27.78	–
144	1.73	29.65	34 [7]

$\Delta\varepsilon/A$, as shown in Figure 2, the effect of high scattering at the hot reservoir becomes prominent. Therefore, more slices near the hot reservoir should be excluded in the simulation sample, which necessitates a larger sample size for reasonably accurate results. In particular, when $\Delta\varepsilon/A$ is quantitatively large, such as 9.80×10^{-4} eV/nm^2 in this case, two states (solid and melting) may occur in the sample during the heat transfer process. Thus, in the remainder of the NEMD simulation work, the value of $\Delta\varepsilon/A$ will be chosen in the range of $1.0 \sim 7.0 \times 10^{-4}$ eV/nm^2 so that the temperature gradients are small enough to ensure the validity of Equation (1).

4. Finite-size effect on thermal conductivity

Finite-size effect arises when the sample length is comparable to the phonon MFP [9]. In this situation, the thermal conductivity of the sample will be limited by its size. This phenomenon is known as the Casimir limit.

We performed the NEMD simulations for various sample lengths, l_z, with the PBC. The sample size is fixed at $2a_0$ in both the x and y directions, but varies from $44a_0$ to $144a_0$ in the z direction. The calculated values of thermal conductivity k for the different sample lengths are shown in Table 1.

It is found that the thermal conductivity depends on the sample length and the heat transfer increases with the sample length. Based on the phonon gas kinetic theory, $k = (1/3)cvl_{\text{eff}}$, the physical mechanism of this dependency can be expressed approximately by the following Equation, [7]:

$$\frac{1}{k} = \frac{a_0^3}{k_B v}\left(\frac{1}{4l_\infty} + \frac{1}{l_z}\right), \tag{6}$$

where $c = (3/2)k_Bn$ is the specific heat of phonons; $n = 8/a_0^3$ is the number density of atoms in the system; $l_{\text{eff}} = (1/l_\infty + 4/l_z)^{-1}$ is the effective MFP; v (≈ 6500 m/s) is the group velocity of an acoustic branch; and l_∞ is the MFP for an infinite bulk system. Equation (6) indicates the linearity between $1/k$ and $1/l_z$.

Based on the simulated results in Table 1, the relationship between k and l_z, and the least-square linear

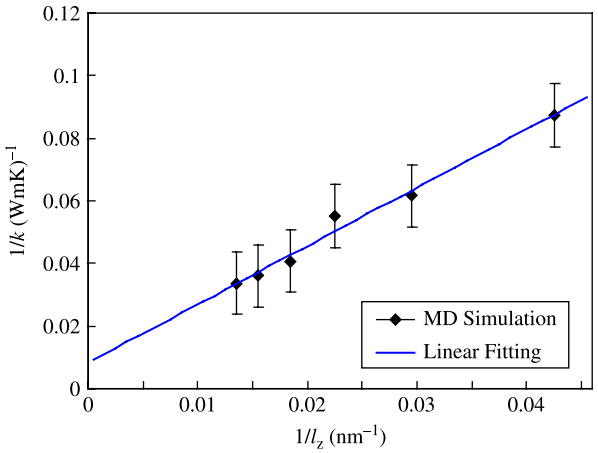

Figure 4. Sample length dependence of $1/k$ on $1/l_z$ at 500 K.

fitting of $1/k$ on $1/l_z$ are extrapolated in Figure 4. It can be observed that $1/k$ and $1/l_z$ have strong linear relationship, which is in accordance with Equation (6). The slope of the linear fitting curve is $1.9 \times 10^{-9}\,\mathrm{m^2\,K/W}$, which is close to the results obtained using the SW potential by Broughton ([10]; $\approx 1.8 \times 10^{-9}\,\mathrm{m^2K/W}$) and Schelling ([7]; $\approx 2.0 \times 10^{-9}\,\mathrm{m^2\,K/W}$). The discrepancy is likely due to the use of different potential models in the NEMD simulations.

Using the linear fitting result, we can also estimate the thermal conductivity of bulk Si by setting $1/l_z = 0$. For instance, $k = 135\,\mathrm{W/mK}$ for the bulk Si at 500 K, which is comparable to 120 W/mK predicted by the experimental data for the isotropically enriched Si at 500 K [11]. The difference between the simulated and experimental results may be attributed to the fact that for the natural Si, defect scattering significantly reduces k, but no defect scattering has been considered in the simulation. Thus, the calculated k is about 10% higher than the experimental value. Based on the extrapolated k, the MFP l_∞ for the bulk Si is estimated as 64 nm at 500 K, which is also reasonable when compared with the reported results of 30 nm at 650 K [11] and 260 nm at room temperature [12].

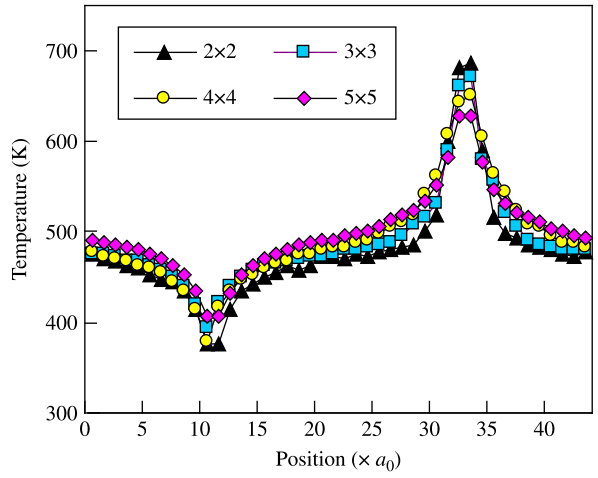

Figure 5. Temperature profiles for the samples with different cross-sectional areas A and same length ($44a_0$) at $T = 500$ K.

Table 2. Comparison of thermal conductivity k for samples with different cross-sectional areas A and same length ($44a_0$).

A ($\times a_0^2$)	$\Delta\varepsilon$ (eV)	∇T_z (K/nm)	k (W/mK)
2×2	4.30	4.48	11.44
3×3	9.68	5.84	8.78
4×4	17.20	7.56	6.78
5×5	26.88	7.52	6.81

Figure 5 illustrates the dependence of k on the cross-sectional area of the samples with the PBC. The results are obtained for the samples with the same length of $44a_0$ but different cross-sectional areas of $2a_0 \times 2a_0$, $3a_0 \times 3a_0$, $4a_0 \times 4a_0$ and $5a_0 \times 5a_0$. The comparison of k obtained from Figure 5 is shown in Table 2. The values of $\Delta\varepsilon$ have been scaled for each different cross-sectional area, so that the heat flux J_z ($\Delta\varepsilon/A \approx 3.65 \times 10^{-4}\,\mathrm{eV/nm^2}$) is the same in each sample. It is apparent that k is less sensitive to the cross-sectional area than to the length and the variations in k are insignificant when the cross-sectional area is larger than $3a_0 \times 3a_0$ for the PBC. It may be attributed to that, for the PBC, phonons are free to travel across the boundaries perpendicular to the heat flux direction without scattering. Physically, the phonons play the role of the carriers of thermal energy, and the propagation of phonons results in energy transport. Hence, changing the cross-sectional area does not remarkably change the scattering and thus the thermal conductivity k.

5. Conclusion

This paper proposed the use of T3 potential for the NEMD simulation of the thermal conductivity of Si nanostructures. The simulated thermal conductivity matched well with the results using the SW potential and the experiment data. The suitability of the Tersoff potential for nanoscale heat transfer simulation was thus validated. In particular, through the comparative study of the NEMD simulations, a reliable range of heat flux for the calculation of thermal conductivity of nanostructures was determined, which provided a useful guideline for choosing suitable values of $\Delta\varepsilon/A$ to simulate the unconventional Si nanostructures/devices with varying cross-sectional areas, such as nano-tips. In addition, since the Tersoff potential has certain advantages in simulating the surface characterization of nanostructures, it is an attractive alternative for simulating the nanoscale structures/devices with unconventional geometries.

Furthermore, the finite-size effect on the thermal conductivity was investigated. The remarkable system length dependence of the thermal conductivity of Si nanostructures was confirmed, which qualitatively may be caused by the factors that the effective phonon MFP is greatly reduced and the number of phonons contributing to the heat transfer or thermal capacity is limited when the length of nanostructures is finite. It is also found that the thermal conductivity is less sensitive to the cross-sectional area perpendicular to the heat flux than to the length. The extrapolated results of thermal conductivity and MFP for the infinite bulk Si system are also comparable to the reported simulated and experimental results.

Notes

1. Email: liux0014@ntu.edu.sg
2. Email: yang_jiaping@dsi.a-star.edu.sg

References

[1] S.J. Cook and P. Clancy, *Comparison of semi-empirical potential functions for silicon and germanium*, Phys. Rev. B 47 (1993), p. 7686.
[2] F.H. Stillinger and T.A. Weber, *Computer simulation of local order in condensed phased of silicon*, Phys. Rev. B 31 (1985), p. 5262.
[3] W.A. Harrison, *Electronic Structure and the Properties of Solids*, Dover, New York, 1989.
[4] R. Biswas and D.R. Hamann, *Interatomic potentials for silicon structural energies*, Phys. Rev. Lett. 55 (1985), p. 2001.
[5] J. Tersoff, *Empirical interatomic potential for silicon with improved elastic properties*, Phys. Rev. B 38 (1988), p. 9902.
[6] B.W. Dodson, *Evaluation of the Stillinger–Weber classical interaction potential for tetragonal semiconductors in nonideal atomic configurations*, Phys. Rev. B 33 (1986), p. 7361.
[7] P.K. Schelling, S.R. Phillpot, and P. Keblinski, *Comparison of atomic-level simulation methods for computing thermal conductivity*, Phys. Rev. B 65 (2002), p. 144306.
[8] P. Jund and R. Jullien, *Molecular-dynamics calculation of the thermal conductivity of vitreous silica*, Phys. Rev. B 59 (1999), p. 13707.
[9] C. Oligschleger and J.C. Schon, *Simulation of thermal conductivity and heat transport in solids*, Phys. Rev. B 59 (1999), p. 4125.
[10] J.Q. Broughton and X.P. Li, *Phase diagram of silicon by molecular dynamics*, Phys. Rev. B 35 (1987), p. 9120.
[11] W.S. Capinski, H.J. Maris, E. Bauser, I. Sillier, M. Asen-Palmer, T. Ruf, M. Cardona, and E. Gmelin, *Thermal conductivity of isotopically enriched SI*, Appl. Phys. Lett. 71 (1997), p. 2109.
[12] G. Chen, *Phonon heat conduction in nanostructures*, Int. J. Thermal Sci. 39 (1999), p. 471.